A 5 GHz Frequency-Tunable SiGe Active Isolator Using a Varactor-Controlled Phase Network

Joseph A. Caezza[#1], Yaw A. Mensah[#], Christopher R. Snyder[#], Alessandro Zerbini[#], Christopher T. Coen[$], John D. Cressler[#]

[#]Georgia Institute of Technology, USA

[$]Georgia Tech Research Institute, USA

[1]caezza@gatech.edu

***Abstract*— This paper presents a novel integrated, frequency-tunable SiGe active isolator. Its high isolation and linearity make it well-suited for communications circuits and other systems that require frequency-agile port isolation. The topology integrates a varactor-based T-network into the feed-forward loop of a traveling-wave isolator, creating a voltage-controlled phase shifter. The fabricated circuit demonstrates a 20 dB isolation tuning range from 4.7 GHz to 5.2 GHz, with an 80 MHz instantaneous bandwidth. The isolator achieves an insertion loss of 0.9 dB, a simulated noise figure of 3.4 dB, and an input-referred P1dB (IP1dB) greater than 30 dBm.**

***Keywords*— Active isolator, tunable isolator, non-reciprocal, phase shifter, directional coupler, Silicon-Germanium (SiGe) heterojunction bipolar transistor (HBT).**

I. Introduction

Isolators are two-port non-reciprocal components used in microwave circuits to allow signal flow only in one direction. They protect sensitive components from spurious RF energy sources, as well as prevent mismatch reflections from affecting other circuit blocks. Commonly, isolators are implemented with magnetic ferrite materials [1], [2], but these types of isolators are bulky and cannot be integrated monolithically with other circuits.

Recently, several MMIC active isolator topologies have demonstrated comparable isolation performance to ferrite isolators. Since active isolators are implemented on-chip, systems can achieve improved performance with reduced size and weight. For example, [3] demonstrated a topology that combines common-base and common-collector transistors. This design achieves wide fractional bandwidth and high isolation, but at the expense of linearity and noise figure. Other designs using resonant structures have been proposed, and while those designs improve linearity, they have very narrow isolation peaks and lack tunability [4]–[7]. In applications where the transmit or receive frequency may change, such as in frequency-agile communications, an isolator with a fixed single-frequency resonant response is not ideal. Frequency-tunable designs are required so that the isolation can be co-tuned with the power amplifier (PA) and antenna.

Traveling-wave designs such as [7], [8] are inherently narrowband since they use phase cancellation. To improve the bandwidth, in the present paper we propose a traveling-wave design, but with the addition of a phase-tuning network, which facilitates an isolation frequency that is electronically-controlled. This frequency-agile combined topology allows for very high linearity, low noise and insertion loss, and high isolation over a wide frequency range.

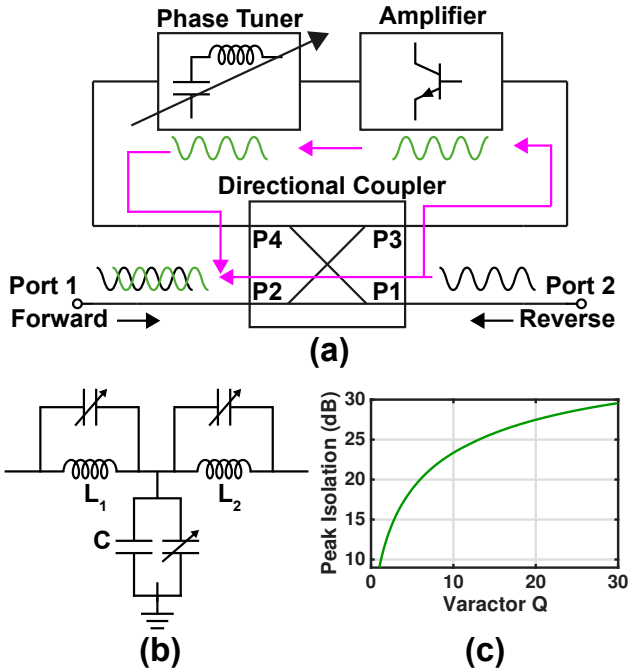

Fig. 1. (a) Circuit block diagram including directional coupler, amplifier, and phase-tuner showing reverse signals destructively interfering. (b) Proposed phase-tuning matching network. (c) Simulated peak isolation of the proposed circuit across varying varactor quality factor at 5 GHz, inductor $Q = 15$.

II. Theory

A. Principle of Operation

A block diagram of the proposed design is shown in Fig. 1(a). The active isolator topology is based on a non-reciprocal feed-forward loop and a directional coupler that has been demonstrated previously in the literature [7], [8]. The principle of operation is based on destructive interference of the reverse-propagating signal.

The Thru path of the isolator is from Port 1 to Port 2, and the isolation path is from Port 2 to Port 1 of the circuit. To illustrate the operation of the isolator, consider

a reverse signal applied to Port 2, as shown in Fig. 1(a). The signal splits, with one part going directly to Port 1 through the Thru path of the coupler. The other part of the signal is coupled into the feedback path and passes through the amplifier and phase-tuning network. When the signals recombine at the output, they are 180 degrees out of phase, and thus destructively interfere. For the forward path, the coupled signal is attenuated by the reverse isolation of the amplifier.

Mathematically, this can be shown by analyzing the scattering matrices of the coupler and feedback path. The S-matrix, $[S]_{DC}$, of a directional coupler with infinite isolation, matched ports, and symmetry is given by

$$[S]_{DC} = \begin{bmatrix} 0 & S_{12} & S_{13} & 0 \\ S_{21} & 0 & 0 & S_{24} \\ S_{31} & 0 & 0 & S_{34} \\ 0 & S_{42} & S_{43} & 0 \end{bmatrix} \tag{1}$$

where the port numbers correspond to the ports shown on the directional coupler in Fig. 1(a).

The combined active non-reciprocal component S-matrix, $[S]_{NC}$, which consists of the amplifier and a phase-tunable network, assuming infinite reverse isolation, is described by

$$[S]_{NC} = \begin{bmatrix} 0 & 0 \\ S'_{21} & 0 \end{bmatrix} \tag{2}$$

As demonstrated in [8], the total S_{12} of the system is

$$S_{12,\text{total}} = S_{12} + \frac{S_{24}S'_{21}S_{31}}{1 - S_{34}S'_{21}} \tag{3}$$

Thus, perfect isolation is achieved when $S_{12,\text{total}} = 0$, so the phase cancellation condition is

$$S_{12} = -\left(\frac{S_{24}S'_{21}S_{31}}{1 - S_{34}S'_{21}}\right) \tag{4}$$

From this it follows that S'_{21} is a critical design parameter for determining optimal isolation. Since the phase of the coupler varies with frequency, previous designs set the phase of this parameter to satisfy (4) at a single frequency.

B. Phase-Tuning Matching Network

The present paper proposes a phase-tunable matching network to increase the frequency range over which the phase cancellation-based isolator can operate. From (4), both the magnitude and phase of S'_{21} determine the amount of isolation. While $|S'_{21}|$ is set by the amplifier and passive losses, with only slight variations from the varactor quality factor, this network, shown in Fig. 1(b), allows control of $\angle S'_{21}$. This means that the frequency of peak isolation can be changed by adjusting the voltage applied to the varactors. The topology is a T-network with two series inductors and a shunt capacitor, as shown in Fig. 1(b). Varactors are placed in parallel with each component to allow for phase tuning.

To analyze the phase response of this network, we first define the parallel combination of the varactors with the inductors and capacitors as effective values

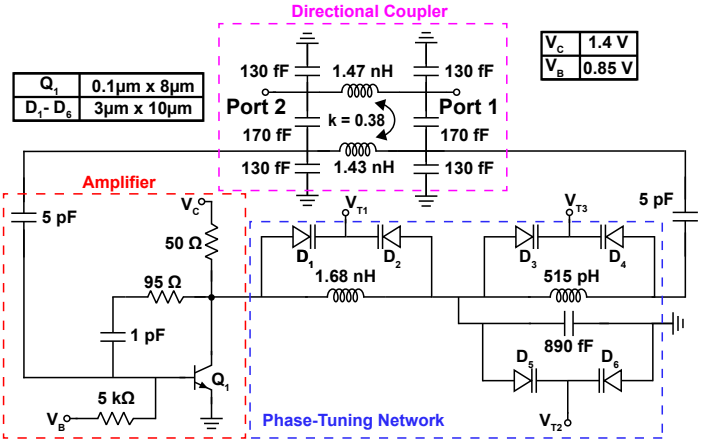

Fig. 2. Schematic of the proposed isolator circuit including lumped-element directional coupler, CE amplifier, and phase-tuning matching network.

$$L_{1_{\text{eff}}}(\omega, V_{\text{T1}}) = L_1/[1 - \omega^2 L_1 C_1(V_{\text{T1}})] \tag{5}$$
$$L_{2_{\text{eff}}}(\omega, V_{\text{T3}}) = L_2/[1 - \omega^2 L_2 C_3(V_{\text{T3}})] \tag{6}$$
$$C_{\text{eff}}(\omega, V_{\text{T2}}) = C + C_2(V_{\text{T2}}) \tag{7}$$

It is then useful to derive the ABCD parameters of the two-port network to calculate the phase. The ABCD parameters, which are functions of frequency and tuning voltage, for this two-port network, can be expressed as

$$A = 1 - \omega^2 L_{1_{\text{eff}}} C_{\text{eff}} \tag{8}$$
$$B = j\omega(L_{1_{\text{eff}}} + L_{2_{\text{eff}}}) - j\omega^3 L_{1_{\text{eff}}} L_{2_{\text{eff}}} C_{\text{eff}} \tag{9}$$
$$C = j\omega C_{\text{eff}} \tag{10}$$
$$D = 1 - \omega^2 L_{2_{\text{eff}}} C_{\text{eff}} \tag{11}$$

The phase of this network is found to be

$$\angle S_{21_{\text{Network}}} = \angle\left(\frac{2}{A + B/Z_0 + CZ_0 + D}\right) \tag{12}$$

which is a function of the tuning voltages, where Z_0 is the characteristic impedance. Finally, the total phase shift of the feedback loop is given by

$$\angle S'_{21} = \angle S_{21_{\text{Amp}}} + \angle S_{21_{\text{Network}}}(V_{\text{T1}}, V_{\text{T2}}, V_{\text{T3}}) \tag{13}$$

Thus, the phase shift of the feedback loop can be changed as a function of the tuning voltages. As a result, the frequency at which (4) is satisfied shifts, moving the peak isolation frequency. The amount of achievable phase change depends on the capacitance range of the specific varactors used.

III. Circuit Design

The proposed circuit schematic is shown in Fig. 2, where a signal entering Port 1 is transmitted to Port 2, and a signal entering Port 2 is isolated from Port 1. The circuit was designed in GlobalFoundries 90 nm SiGe BiCMOS technology [10]. Since the designed center frequency was 5 GHz, coupled

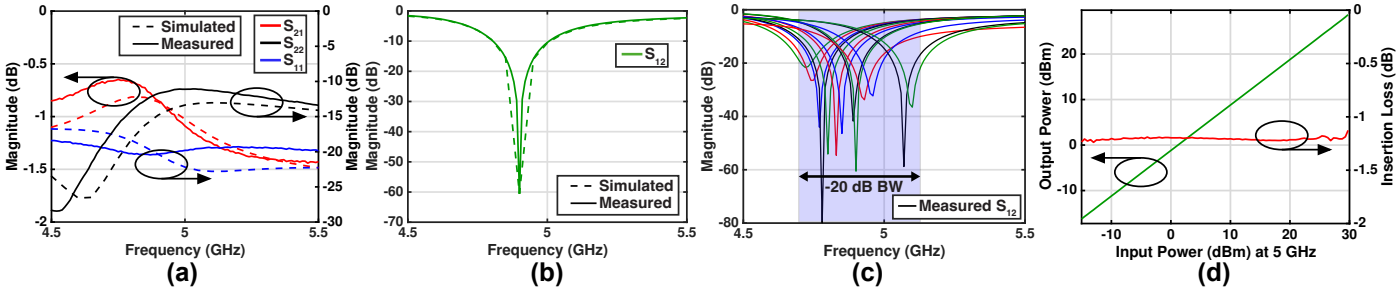

Fig. 3. (a) Measured and simulated matching and forward insertion loss (S_{21}) at $V_{T1} = 2.4\,\text{V}$, $V_{T2} = 3.2\,\text{V}$, and $V_{T3} = 0.8\,\text{V}$. (b) Measured and simulated reverse isolation (S_{12}) at $V_{T1} = 2.4\,\text{V}$, $V_{T2} = 3.2\,\text{V}$, and $V_{T3} = 0.8\,\text{V}$. (c) Measured reverse isolation of the isolator across tuning voltages illustrating a 20 dB isolation tuning bandwidth of 4.7 GHz to 5.2 GHz. (d) Insertion loss and output power across input power up to 30 dBm at 5 GHz.

Table 1. Performance Comparison of Integrated Isolators

Parameter	[3]	[8]	[9]	[4]	**This Work**
Technology	200 nm SiGe	180 nm CMOS	65 nm CMOS	130 nm SiGe	**90 nm SiGe**
Center Frequency (GHz)	5–6	24	90/100/105	210	**4.95**
IL (dB)	2	1.8	4.5	1.4	**0.9**
Inst. Iso. BW (GHz)‡	1 (18%)	0.3 (1.2%)	10 (11%)	0.2 (0.10%)	**0.08 (1.6%)**
Tuning Range (GHz)	–	–	–	–	**4.7–5.2**
NF (dB)	13	6†	4.53†	6.6†	**3.41**†
IP1dB (dBm)	-8.3*	NR§	10.9†	NR§	**>30**§
P_{dc} (mW)	5.4	3.6	9.6–12.9	6	**4.8**
Active Area (mm^2)	0.070	0.228	0.245	0.037	**0.179**

†Simulation results; ‡instantaneous bandwidth with isolation $\geq$20 dB (fractional bandwidth in parentheses); *estimated from reported results; §IP1dB compression point not reached within the available input power range.

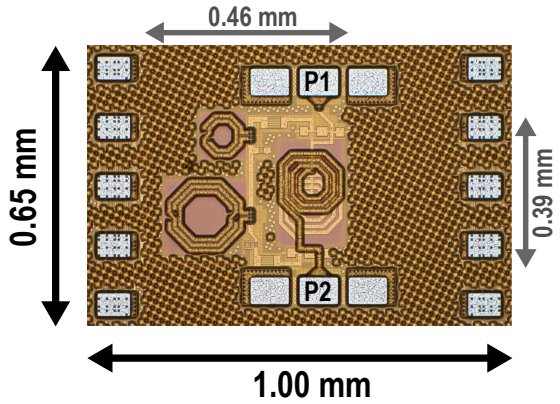

Fig. 4. Die micrograph of the SiGe isolator.

lines and transmission lines would be very large for an on-chip directional coupler. Therefore, a lumped-element directional coupler was used in order to maximize area efficiency. The coupler uses a conventional topology, with coupled inductors and several capacitors, as shown at the top of Fig. 2. The coupling was designed to be −7.3 dB, and is the result of a trade-off between forward insertion loss and coupling. The amplifier compensates the added attenuation in the feedback path to satisfy (4).

The common-emitter (CE) amplifier was designed to meet the condition in (4). The device was biased to provide a reverse isolation of 20 dB and a gain of 2.5 dB, which is needed to cancel the passive losses of the feedback loop and coupler Thru path. Resistive feedback was used to ensure flat gain response across the desired frequency range, as any magnitude deviations would limit the achievable bandwidth from the tuning network.

An important consideration for the tunable matching network described in Section II-B is the selection of varactors. The varactor quality factor has a large impact on the isolation performance. Fig. 1(c) shows the effect on isolation across a sweep of the varactor quality factor at 5 GHz. The circuit's peak isolation drops precipitously at low varactor quality factors, since the increased network loss moves S'_{21} away from the cancellation condition in (4). As a result, high-Q varactors are critical for the design.

The hyperabrupt varactors offered in this SiGe platform were chosen for the implementation of the T-network in this design. The quality factor obtained from the hyperabrupt varactors was about 20. While this moderate quality factor may degrade peak isolation, the hyperabrupt varactors have a relatively large capacitance tuning range of about 200 fF, which makes them the best available option for the design.

IV. Measurement Results

The circuit was fabricated and measured on-wafer to verify the isolator performance and operation of the tunable matching network. A die micrograph of the fabricated circuit is shown in Fig. 4. The circuit consumes a quiescent power of 4.8 mW.

The small-signal S-parameters were measured with a Keysight E8363B PNA. To assess measurement and simulation agreement, the center tuning point was selected where $V_{T1} = 2.4\,\text{V}$, $V_{T2} = 3.2\,\text{V}$, and $V_{T3} = 0.8\,\text{V}$. Results for the matching and insertion loss are shown in Fig. 3(a), and the isolation is shown in Fig. 3(b). Overall, the measurement and simulation results agree well. Across the tuning range, the simulated noise figure remains low and is 3.4 dB at the isolation peak as shown in Fig. 5.

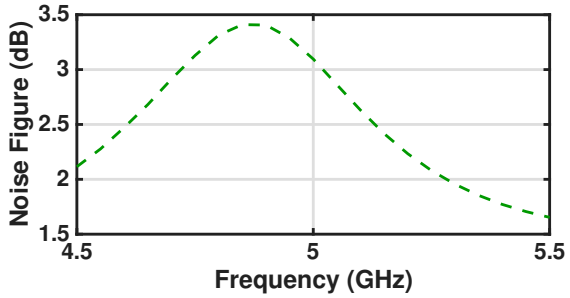

Fig. 5. Simulated noise figure at $V_{T1} = 2.4\,\text{V}$, $V_{T2} = 3.2\,\text{V}$, and $V_{T3} = 0.8\,\text{V}$.

All three tuning voltages were swept from 0.5 V to 4 V in 0.1 V increments to fully characterize the frequency tuning range. A subset of the measured isolation curves is shown in Fig. 3(c), where the curve with the best isolation was chosen in 25 MHz increments. The measured 20 dB isolation range of the isolator over the swept tuning bias is 4.7 GHz to 5.2 GHz, with an 80 MHz instantaneous bandwidth across the range.

Because the forward path passes only through the passive coupler, the active devices reside solely in the reverse cancellation path, so the forward-path IP1dB of the circuit is theoretically very high. This was experimentally verified up to 30 dBm, our instrumentation limit. The large-signal measurements were conducted using a Keysight E8257D Signal Generator connected to an ATN Microwave Power Amplifier Module that drove the input of the circuit. The output of the circuit was connected to an attenuator to protect the Keysight E4446A Spectrum Analyzer used to measure the output power. Probe, cable, and attenuator losses were de-embedded to measure the output power accurately. Fig. 3(d) shows that the circuit is linear up to 30 dBm of input power.

A performance comparison to the prior art is shown in Table 1. Direct comparison is difficult due to the disparate operating frequencies in the existing literature. Because the forward path passes only through the passive coupler, the present work achieves the lowest insertion loss and highest measured IP1dB. The noise figure and power consumption are also competitive for the operating frequency. While the instantaneous bandwidth is narrow, this work is the only one with continuously tunable isolation over frequency, which effectively extends the usable bandwidth.

V. Summary

A high-performance, frequency-tunable active isolator has been designed and demonstrated in 90 nm SiGe BiCMOS technology. This work overcomes the fixed-frequency limitation of prior resonant isolators by incorporating a novel varactor-based T-network, which functions as a voltage-controlled phase shifter in the active feed-forward loop. The circuit achieves tunable 20 dB isolation from 4.7 GHz to 5.2 GHz with an 80 MHz instantaneous bandwidth across the range. The circuit has an insertion loss of 0.9 dB, a power consumption of 4.8 mW, and an IP1dB exceeding 30 dBm.

Acknowledgment

The authors would like to thank the GlobalFoundries SiGe team for chip fabrication and the members of the Silicon-Germanium Devices and Circuits team for technical discussions. The authors would also like to acknowledge the GTRI CTO's Office and Chief Scientists for funding this work under IRAD.

References

[1] B. Lax and K. J. Button, *Microwave Ferrites and Ferrimagnetics*. McGraw-Hill, 1962.

[2] J. D. Adam, L. E. Davis, G. F. Dionne, E. F. Schloemann, and S. N. Stitzer, "Ferrite devices and materials," *IEEE Trans. Microw. Theory Techn.*, vol. 50, no. 3, pp. 721–737, Mar. 2002.

[3] J. Lee, J. D. Cressler, and A. J. Joseph, "A 5–6 GHz SiGe HBT monolithic active isolator for improving reverse isolation in wireless systems," *IEEE Microw. Wireless Compon. Lett.*, vol. 15, no. 4, pp. 220–222, Apr. 2005.

[4] Y. Wang, W. Chen, and X. Li, "A 210 GHz magnetless nonreciprocal isolator in 130-nm SiGe BiCMOS based on resistor-free unidirectional ring resonators," *IEEE Microw. Wireless Compon. Lett.*, vol. 30, no. 5, pp. 524–527, May 2020.

[5] Y. Wang, W. Chen, X. Li, S. Li, and P. Zhou, "305–325 GHz non-reciprocal isolator based on peak-control gain-boosting magnetless non-reciprocal metamaterials," in *2021 IEEE Radio Frequency Integrated Circuits Symposium (RFIC)*, 2021, pp. 47–50.

[6] S. Masui, T. Kojima, Y. Uzawa, and T. Onishi, "A novel microwave nonreciprocal isolator based on frequency mixers," *IEEE Microw. Wireless Technol. Lett.*, vol. 33, no. 7, pp. 1051–1054, Jul. 2023.

[7] M. Muraguchi, K. Araki, and Y. Naito, "A new type of isolator for millimeter-wave integrated circuits using a nonreciprocal traveling-wave resonator," *IEEE Trans. Microw. Theory Techn.*, vol. 30, no. 11, pp. 1867–1873, Nov. 1982.

[8] J.-F. Chang, J.-C. Kao, Y.-H. Lin, and H. Wang, "A 24 GHz fully integrated isolator with high isolation in standard RF 180-nm CMOS technology," in *2014 IEEE MTT-S International Microwave Symposium (IMS2014)*, 2014, pp. 1–3.

[9] C. Yang and P. Gui, "85–110 GHz CMOS magnetic-free nonreciprocal components for full-duplex transceivers," *IEEE J. Solid-State Circuits*, vol. 54, no. 2, pp. 368–379, Feb. 2019.

[10] U. S. Raghunathan *et al.*, "Performance improvements of SiGe HBTs in 90nm BiCMOS process with fT/fmax of 340/410 GHz," in *2022 IEEE BiCMOS and Compound Semiconductor Integrated Circuits and Technology Symposium (BCICTS)*, 2022, pp. 232–235.